Research Square

Preprints are preliminary reports that have not undergone peer review.
They should not be considered conclusive, used to inform clinical practice,
or referenced by the media as validated information.

Rumen metagenomics of Tan sheep with divergent growth rate: functional gene and MAG profiles do not distinguish the groups

Jin Wang[1]
wangjin8208@163.com

Ningxia Academy of Agriculture and Forestry Sciences

Yu Fan[1]
Ningxia University

Huiming Zhang[1]
Ningxia University

Jifeng Ma[1]
Ningxia Academy of Agriculture and Forestry Sciences

Qing Ma[1]
Ningxia Academy of Agriculture and Forestry Sciences

Xuansheng Li[1]
Ningxia Agricultural Reclamation Beef and Lamb Food Co., Ltd.

Research Article

Keywords: Tan sheep, feed conversion ratio, average daily gain, rumen metagenome, metagenome-assembled genome, carbohydrate transport, nested cross-validation, permutation test, candidate gene panel

Posted Date: November 4th, 2026

DOI: https://doi.org/10.21203/rs.3.rs-11079559/v1

License: This work is licensed under a Creative Commons Attribution 4.0 International License. Read Full License

Additional Declarations: No competing interests reported.

Abstract

Background

Feed conversion ratio (FCR) is a key economic trait in lamb production, and the rumen microbiome governs the energy the host obtains from feed. Because genus-level biomarkers are inconsistent across studies, we examined whether efficient and inefficient Tan sheep differ at the level of metabolic genes and metagenome-assembled genomes (MAGs). Sixteen Tan sheep, drawn from a finishing cohort of 100 animals, were ranked by average daily gain (ADG) and split into a high-growth/low-FCR group (n = 10) and a low-growth/high-FCR group (n = 6); individual feed intake was not recorded, so ADG, not measured FCR, defined the groups. Rumen contents were deep-shotgun sequenced, assembled and binned. Of 3,283 retained KEGG orthologues (KOs), a candidate required both a Wilcoxon between-group difference ($P < 0.05$) and a Spearman ADG correlation ($P < 0.05$) with concordant direction, because no adjusted P reached 0.05 (smallest Benjamini-Hochberg-adjusted P = 0.41). Because the two layers are not independent - the groups were formed by ranking the same ADG values - we calibrated the size of the resulting candidate set against a label-permutation null distribution, and we evaluated a Lasso-plus-logistic-regression classifier under nested leave-one-out cross-validation, in which feature selection was repeated inside every fold and the permutation test re-ran the entire pipeline.

Results

Global community structure did not differ (ANOSIM taxonomy R = -0.139, P = 0.95; function R = -0.064, P = 0.682). The two-layer screen yielded 36 direction-concordant KOs (54 between-group and 94 ADG-correlated; union 112), enriched for sugar-transport (ABC/PTS) and energy genes, whereas canonical VFA genes showed no detectable difference (buk, pct, acs; all $P > 0.7$; absence of evidence rather than evidence of absence). However, 36 double-evidence KOs did not exceed the label-permutation null expectation (null mean 67, 95th percentile 195; P = 0.59), and the same was true for each single layer (between-group: 54 observed versus null mean 131, P = 0.83; ADG-correlated: 94 observed versus null mean 167, P = 0.67). A classifier built on the 36 KOs and evaluated with the feature set fixed in advance reached AUC = 1.000 and 87.5% accuracy, but under nested cross-validation the same pipeline gave AUC = 0.767 and 56.2% accuracy (9/16), which did not differ significantly from the permutation null (null mean AUC = 0.525, 95th percentile 0.883; P = 0.190). Initial body weight was confounded with group (Spearman rho with ADG = 0.67, P = 0.005). Only three MAGs were double-evidence, all inefficient-enriched and negatively correlated with ADG, representing unnamed novel genera (two Firmicutes-affiliated and one Bacteroidota-affiliated).

Conclusions

In this cohort of 16 Tan sheep, growth-efficiency divergence was not accompanied by any statistically detectable remodelling of rumen functional genes: the carbohydrate-uptake and energy-metabolism candidate panel did not exceed permutation-based null expectations, no KO approached FDR significance, and no classifier generalised under nested validation. The 591 MAGs recovered here provide a breed-specific genome resource for Tan sheep, and the contrast between the non-nested (AUC = 1.000) and nested (AUC = 0.767) estimates quantifies how much apparent signal feature selection performed outside cross-validation can manufacture at this sample size.

Introduction

Feed conversion ratio (FCR), usually expressed as kilograms of feed consumed per kilogram of live-weight gain, directly determines the profitability and environmental footprint of lamb production. In mutton systems based on Tan sheep, an indigenous Chinese sheep breed of major economic importance, even small improvements in the efficiency with which ingested feed is converted into edible tissue translate into large savings of concentrated feed and reduced methane and nitrogen excretion. Recent integrative work in Hu sheep has confirmed that gut microbial, host-transcriptomic and blood-metabolomic features covary with FCR [1], and multi-omics studies in sheep more broadly have implicated the rumen microbiome as a central regulator of feed efficiency [2]. Quantifying the microbial functional basis of these differences is therefore a practical prerequisite for selecting or managing animals for higher efficiency.

The rumen is a fermentation vat in which anaerobic microorganisms convert plant biomass into volatile fatty acids (VFAs) and microbial protein, the two dominant sources of energy and amino acids for the host. Because the host is largely unable to access the energy locked in fibrous plant material, the composition and metabolic capacity of the rumen microbiome set an upper bound on the energy that can be harvested from a given diet. Landmark studies have demonstrated that efficient ruminants harbour microbiomes that differ in energy-harvesting capacity [3, 4], and that even at the community level high- and low-efficiency steers can be distinguished by ruminal bacterial composition [5]. These observations established the conceptual basis for a microbiome-mediated contribution to host feed efficiency.

Metagenomics has deepened this picture. Early surveys recovered numerous biomass-degrading glycoside hydrolases and genomes directly from the cow rumen [6, 7], and later gene- and genome-centric studies repeatedly linked efficient animals to enriched ABC and phosphotransferase (PTS) transporters, two-component regulatory systems and amino-acid biosynthetic pathways across breeds and species [8–11]. Integrated meta-omics further identified carbohydrate and pathway-level features that discriminate efficient dairy cows [12]. A persistent and well-recognized problem, however, is taxonomic inconsistency: the bacterial genera (for example Prevotella, Succinivibrionaceae or

Ruminococcaceae) reported as enriched in efficient animals differ across diets, breeds, laboratories and host species, and several seminal studies found that overall community structure did not differ between efficiency groups even when functional signatures did [3, 4, 11]. Predictive and machine-learning approaches have therefore shifted attention from genus-level labels to robust microbial genes and genomes [13–15].

Despite this progress, gene- and genome-centric evidence for feed-efficiency divergence remains heavily weighted to cattle, and much of it is correlative and cross-sectional. Whether a small, directionally consistent set of functional modules, rather than global community change or a named genus, distinguishes efficient from inefficient ruminants is unresolved. We therefore asked whether growth-efficiency divergence in finishing Tan sheep is concentrated in a limited number of rumen microbial functional modules, principally those governing carbohydrate uptake and energy metabolism, and whether such differences are detectable at the metabolic-gene level when overall community structure and canonical VFA-production genes are indistinguishable. Because 16 animals is small relative to the 3,283 features tested, we pre-specified that a null outcome would be interpreted with an explicit statistical power analysis and a label-permutation calibration, and that any classifier would be evaluated under nested cross-validation. To test this, we deep-shotgun sequenced rumen metagenomes from Tan sheep divergent in ADG, applied a conservative two-layer screening strategy (between-group difference and phenotype correlation with concordant direction), derived metagenome-assembled genomes, and ranked candidate genes by a bootstrapped machine-learning model.

Materials and Methods

Animals and experimental design, phenotyping and grouping

Sixteen healthy, intact (uncastrated) male Tan sheep, weaned at 3 months of age, were raised on the experimental farm of Ningxia Nongken Tan Sheep Industry Co., Ltd. (Nuanquan Sheep Farm; approval no. NXU-2025-309) under a single, standardized finishing regimen. The total mixed ration (TMR), offered twice daily with free access to water, was formulated on a dry-matter (DM) basis with corn stalk 17.53%, corn cob 13.38%, Caragana korshinskii 9.09%, corn 36.00%, corn dried distillers' grains with solubles 7.00%, wheat middlings 5.00%, soybean meal 3.50%, cottonseed meal 5.00%, dicalcium phosphate 1.00%, limestone 1.00%, premix 1.00% and NaCl 0.50%, providing (DM basis) 9.61 MJ/kg metabolizable energy, 14.10% crude protein, 42.86% neutral detergent fibre, 1.11% Ca and 0.61% total P (air-dry DM 86.78%). Average dry-matter intake was approximately 1.37 kg/d (1,576 g/d on an air-dry basis). Body weight was recorded at the start and end of the 59-d feeding trial, and average daily gain (ADG, g/d) was calculated as the difference between final and initial body weight divided by trial length. Individual feed intake was not recorded per lamb; because all animals received the same TMR with negligible between-pen intake variation, ADG (rather than FCR) was used to define efficiency groups under iso-intake conditions (higher ADG corresponds to lower FCR). Throughout the manuscript we therefore treat ADG as the measured phenotype and FCR as a derived, descriptive quantity. The two groups also differed in initial body weight (Table 1), which we treat explicitly as a potential confounder rather than as part of the phenotype (see Statistical analysis). Pen identity and batch records were not retained at the individual level, so pen effects cannot be excluded; all 16 animals were, however, managed under one standardized regimen in the same facility over the same period. For descriptive purposes, estimated FCR (kg DM intake per kg gain) was computed as DMI divided by ADG using the pen-level mean DM intake (1.368 kg/d) for all animals, yielding ranges of 3.87–4.55 and 6.90–8.63 kg DM/kg gain in the low- and high-FCR groups, respectively. These 16 animals were drawn from a finishing cohort of 100 Tan sheep managed contemporaneously under the same standardized regimen, and were ranked by ADG and allocated retrospectively into two phenotypically divergent groups: a low-FCR (high-efficiency) group of 10 lambs (LW082, LW113, LW049, LW091, LW017, LW021, LW044, LW015, LW108, LW022) and a high-FCR (low-efficiency) group of 6 lambs (LW089, LW027, LW077, LW006, LW051, LW042). The two groups did not overlap in ADG (300.9-353.4 versus 158.5-198.3 g/d), separated by a gap of 102.5 g/d. Because animals were selected from the two tails of a larger cohort rather than sampled at random, any microbial difference attributable to growth rate estimated here is a contrast between phenotypic extremes; such contrasts are expected to exceed those in an unselected population and should not be read as population-average effect sizes. All 16 animals completed the 59-day trial and were included in the analysis; no animal died, required treatment for disease, or was excluded. Because group allocation was retrospective - animals were ranked by ADG only after the trial - rumen sampling, DNA extraction, library preparation and sequencing were all completed before any group label existed, and could not have been blinded to it; no blinding was applied during the subsequent statistical and bioinformatic analyses.

Sampling and shotgun sequencing

Rumen contents were collected immediately after slaughter, homogenized, aliquoted and stored at -80°C until processing. Total DNA was extracted from approximately 200 mg of rumen digesta using a commercial metagenomic DNA-extraction kit following the manufacturer's instructions, and sequencing libraries were constructed with a paired-end library-preparation kit. Total DNA was subjected to Illumina paired-end shotgun sequencing (2 x 150 bp; Tsingke Biotechnology Co., Ltd., Beijing, China), yielding 6.20–9.42 Gb of clean data per sample (GC content 37.8–50.3%; Q20 99.58–99.76%; Q30 98.01–98.82%) after removal of adapter-contaminated reads and low-quality reads with fastp v0.23.0 [37] (reads containing > 10% N bases, or reads in which bases with Q < = 10 accounted for > = 50% of the read, were discarded).

Read processing, assembly, gene catalogue and functional/taxonomic annotation

Host-derived reads were identified by alignment against an Ovis aries reference genome using bowtie2 v2.5.3 [35] and removed. The sequencing provider did not record which Ovis aries assembly was indexed; because host-derived reads accounted for only 0.0005–0.081% of raw reads (median 0.004%) and 99.62–99.97% of raw bases were retained as clean data (Supplementary Table S3), neither the choice of assembly nor the alignment stringency can materially affect any result reported here, and host contamination was negligible. The remaining clean reads were co-assembled with MEGAHIT v1.2.9 [16]; contigs of > = 500 bp were retained. Genes were predicted with Prodigal v2.6.3 [33], and ORFs were dereplicated with CD-HIT v4.8.1 [34] at 95% sequence identity and 90% coverage to obtain a non-redundant gene catalogue of 2,729,000 genes with a mean length of 759.8 bp. Per-gene abundance was quantified by mapping clean reads back to the gene catalogue with bowtie2 v2.5.3 [35] (95% identity) and expressed as transcripts per million (TPM). Taxonomic assignment of genes was performed by lowest-common-ancestor (LCA) against the NCBI non-redundant (NR) database (version 2023-08-30) using DIAMOND v2.0.13 [36] (blastp, E-value < = 1e-5). Functional annotation used DIAMOND against the KEGG orthology (release 2023-08-30), eggNOG [17] and CAZy (v8) databases (E-value < 1e-5; the single highest-scoring HSP with > 60 bits was retained).

Metagenome-assembled genomes

Bins were generated with the deep-variational-autoencoder binner VAMB [18], following established genome-resolved metagenomic practices [25]. Bin quality was assessed with CheckM v1.0.12 [19], and only metagenome-assembled genomes (MAGs) with completeness > 50% and contamination < 10% were retained, following the quality framework established for large rumen genome catalogues [20]. Taxonomic classification of MAGs was performed with the Genome Taxonomy Database toolkit (GTDB-Tk v1.7.0) against GTDB release 202 (r202).

Statistical analysis of KO and MAG abundance

Of 3,757 annotated KOs, 3,283 (TPM > 0 in at least 4 of 16 samples) were tested. For each KO, between-group abundance differences were assessed with the two-sided Mann-Whitney-Wilcoxon test, and Spearman rank correlation between abundance and ADG was computed across all 16 animals. P values were adjusted for multiple testing by the Benjamini-Hochberg (BH) procedure; the smallest adjusted P was 0.41 for the between-group test and 1.00 for the ADG correlation, so no KO reached FDR significance. We therefore used the pre-specified two-layer framework as a ranking device: a KO was retained as a candidate when it was (i) between-group significant (P < 0.05) AND (ii) significantly associated with ADG (P < 0.05) AND (iii) the between-group log2 fold change and the ADG correlation had concordant signs. We do not treat these two layers as independent evidence: the groups were formed by ranking the same ADG values, so the between-group test and the ADG correlation are two views of one signal, and their intersection cannot be interpreted as replication. To calibrate the framework, we therefore built a label-permutation null distribution: group membership and ADG were permuted together 200 times (preserving the 10/6 split), the full two-layer screen was repeated on each permutation, and the number of candidates at each layer was recorded; the empirical P value is the proportion of permutations yielding at least as many candidates as observed. Because log2 fold changes computed with a small pseudo-count are unstable when a group median is zero (which generated apparent log2FC values near +/-19 in an earlier version), fold changes are now reported with a pseudo-count of 1 TPM and are accompanied by per-group detection rates (number of animals with TPM > 0) and by the number of catalogue genes supporting each KO. Confounding by initial body weight was assessed by Spearman correlation of every candidate KO with initial weight and by comparing its effect size with that of ADG. Overall community separation was tested by ANOSIM on Bray-Curtis distances separately for taxonomic and functional profiles, complemented by permutational multivariate analysis of variance (PERMANOVA, 999 permutations) and a test of multivariate dispersion (betadisper). The same two-layer criterion and permutation calibration were applied to the 591 qualified MAGs. Statistical power. Because the primary outcome was null, we quantified the effect sizes this design could detect. For each KO we estimated the pooled within-group standard deviation of log2(TPM + 1) abundance (median 0.75), then simulated two-group comparisons by drawing 200 replicates for each of 300 randomly sampled KOs under log2 fold changes equivalent to 1.5-, 2-, 3- and 4-fold differences, at the realised design (10 versus 6) and at hypothetical designs of 16 + 16, 24 + 24, 40 + 40 and 48 + 48 animals, and recorded the proportion of replicates reaching P < 0.05 and P < 0.05/3,283 (Bonferroni).

Machine-learning classification and feature ranking

The 112 KOs in the union of the two single-layer screens were used to build a classification model of ADG group. Lasso-regularized logistic regression (coordinate-descent solver) was run over 30 bootstrap resamples to obtain per-KO selection frequency; KOs selected in at least 30% of bootstraps were defined as high-frequency features. For performance estimation we used nested leave-one-out cross-validation: in each of the 16 outer folds the held-out animal was removed first, the two-layer screen was re-run on the remaining 15 animals, the at most 20 top-ranked candidates (ranked by the product of the two P values) were carried forward, centred-log-ratio transformation and standardization were fitted on the training animals only, and an L2-penalized logistic-regression model was fitted and applied to the held-out animal. No step of feature selection, transformation or scaling ever saw the held-out animal. The AUC was computed from the held-out predictions using the equivalence between the ROC AUC and the Mann-Whitney U statistic. To quantify how much apparent signal is created when the feature set is instead

selected on all animals before cross-validation, we repeated the identical procedure with a fixed, globally selected feature set as a non-nested control. For inference, group labels and ADG were permuted together 1,000 times and the complete nested pipeline, including feature selection, was re-run on each permutation; the empirical P value is the proportion of permutations reaching an AUC at least as large as observed. We report the nested estimate as the primary result and the non-nested estimate only as a methodological control.

Results

Growth phenotypes and grouping

The 16 lambs formed two non-overlapping phenotype classes (Table 1). The high-growth (low-FCR) group gained on average 18.99 +/- 1.04 kg over the trial and had a mean ADG of 321.86 +/- 17.71 g/d (range 300.85-353.39 g/d), whereas the low-growth (high-FCR) group gained 10.55 +/- 0.99 kg with a mean ADG of 178.81 +/- 16.80 g/d (range 158.47-198.31 g/d). Estimated FCR (pen-level DM intake divided by ADG) averaged 4.26 +/- 0.23 kg DM/kg gain in the low-FCR group (range 3.87–4.55) versus 7.71 +/- 0.73 kg DM/kg gain in the high-FCR group (range 6.90–8.63). Initial body weight was 31.51 +/- 3.20 kg (low-FCR) versus 26.92 +/- 3.47 kg (high-FCR), and final body weight was 50.50 +/- 3.82 kg versus 37.48 +/- 3.67 kg. Two features of this contrast qualify its interpretation. First, no animal had an ADG between 198 and 301 g/d, so the two groups are separated by a gap rather than drawn from a continuous distribution; under a common diet this pattern is compatible with, but not proof of, a genuine efficiency dichotomy, and it is also compatible with unrecorded differences in intake, age or pen. Second, initial body weight was itself correlated with ADG (Spearman rho = 0.67, P = 0.005) and differed between groups, so part of any microbial contrast could track body size or developmental stage rather than feed conversion efficiency. We therefore treat ADG as the primary phenotype, carry initial weight forward as an explicit confounder, and do not claim that the groups differ in measured FCR.

Table 1
Per-animal growth phenotypes of the 16 Tan sheep. Estimated FCR is a derived quantity (pen-level mean DM intake of 1.368 kg/d divided by individual ADG) and was not measured; individual feed intake was not recorded.

Animal ID	Sample ID	Group	Initial BW (kg)	Final BW (kg)	Weight gain (kg)	ADG (g/d)	Estimated FCR (kg DM/kg gain)
82	LW082	LFCR	33.30	54.15	20.85	353.39	3.87
113	LW113	LFCR	34.00	54.55	20.55	348.31	3.93
49	LW049	LFCR	31.50	51.15	19.65	333.05	4.11
91	LW091	LFCR	31.90	50.85	18.95	321.19	4.26
17	LW017	LFCR	31.40	50.30	18.90	320.34	4.27
21	LW021	LFCR	35.65	54.15	18.50	313.56	4.36
44	LW044	LFCR	34.95	53.40	18.45	312.71	4.37
15	LW015	LFCR	25.70	43.90	18.20	308.47	4.43
108	LW108	LFCR	28.55	46.65	18.10	306.78	4.46
22	LW022	LFCR	28.15	45.90	17.75	300.85	4.55
89	LW089	HFCR	27.55	39.25	11.70	198.31	6.90
27	LW027	HFCR	29.95	41.55	11.60	196.61	6.96
77	LW077	HFCR	25.05	35.75	10.70	181.36	7.54
6	LW006	HFCR	23.10	33.50	10.40	176.27	7.76
51	LW051	HFCR	24.05	33.60	9.55	161.86	8.45
42	LW042	HFCR	31.85	41.20	9.35	158.47	8.63

Global community and functional structure did not differ between groups

Despite the pronounced growth-phenotype contrast, the overall rumen communities of the two groups were indistinguishable. ANOSIM on taxonomic profiles gave R = -0.139 (P = 0.95), and on functional profiles R = -0.064 (P = 0.682): neither statistic indicated a separation between efficiency groups. Consistent with earlier reports, this result shows that divergent feed efficiency in this cohort was not reflected in a wholesale shift of community composition or functional repertoire at the profile level, and that any associated signal would be expected at the level of individual genes and genomes.

Two-layer screening identifies 36 double-evidence candidate KOs

Of the 3,283 tested KOs, 54 differed significantly between the low- and high-FCR groups (Wilcoxon $P < 0.05$) and 94 were significantly correlated with ADG (Spearman $P < 0.05$). The union contained 112 KOs and the direction-concordant intersection contained 36 candidates. Hierarchical clustering of the 36 candidates separated the two phenotype groups (heat map in Fig. 2). These candidates were enriched for sugar transport and central energy metabolism, and we list them in Table 2 as a prioritized resource for targeted validation. Their statistical status, however, is nominal only. Under the label-permutation null, the between-group layer alone yielded a mean of 131 KOs at $P < 0.05$ (95th percentile 314), the ADG layer a mean of 167 (95th percentile 406), and the two-layer intersection a mean of 67 (95th percentile 195); the observed counts (54, 94 and 36) were therefore not larger than expected under the null ($P = 0.83$, 0.67 and 0.59, respectively). The permutation distribution is also extremely dispersed, because the 3,283 KOs are strongly inter-correlated: a single random relabelling that happens to align with a dominant compositional gradient can produce several hundred nominally significant KOs. Direction concordance is likewise not independent evidence, because concordance was part of the selection rule. We therefore report the 36 KOs as a nominal, hypothesis-generating ranking and not as a set of FDR-level or permutation-calibrated discoveries. One candidate, K06237 (COL4A, collagen type IV alpha), is a metazoan extracellular-matrix gene supported by a single catalogue gene with no binned MAG and detected in only one animal; it almost certainly reflects residual host DNA or misannotation, is retained in Table 2 only for completeness and is excluded from interpretation. Several further candidates (for example K17246 and K10780) rest on a single supporting gene, which is why per-KO gene support and detection rates are now reported in Table 2 and should be used when prioritising targets for validation.

Table 2

The 36 nominal candidate KOs grouped by functional module, with group log2 fold change (low-FCR/high-FCR; pseudo-count 1 TPM), between-group Wilcoxon P, ADG Spearman rho and P, Lasso bootstrap selection frequency, per-group detection rate (animals with TPM > 0 of 10 and 6) and the number of catalogue genes supporting each KO. Fold changes for KOs supported by one or two genes should be interpreted with caution.

Module	KO	Annotation	log2FC	P(group)	rho_ADG	P(ADG)	Lasso freq.	Supporting genes (n)	Detection (low-FCR/high-FCR)
Carbohydrate utilization	K17246	chiG, chitobiose ABC permease	0.60	0.032	0.62	0.010	73.3%	1	9/2
VFA/energy	K10780	fabL, enoyl-ACP reductase III	-0.94	0.003	-0.68	0.004	66.7%	1	2/6
Carbohydrate utilization	K10984	agaB, galactosamine PTS EIIB	0.21	0.027	0.73	0.001	50.0%	n.a.	8/1
Amino-acid/vitamin	K00303	soxB, sarcosine oxidase beta	0.70	0.007	0.71	0.002	36.7%	7	10/6
Carbohydrate utilization	K01612	bsdC, vanillate decarboxylase subunit C	0.29	0.029	0.57	0.020	36.7%	n.a.	6/0
Transport/two-component/N	K07709	zraS/hydH, sensor histidine kinase	-0.88	0.010	-0.6	0.014	36.7%	n.a.	5/6
VFA/energy	K20451	mii, methylitaconate Delta-isomerase	0.48	0.015	0.62	0.011	30.0%	n.a.	8/1
Amino-acid/vitamin	K01556	kynU, kynureninase	-0.05	0.009	-0.59	0.016	26.7%	n.a.	1/5
Host/drug-resistance/secretion	K08777	nprB, neutral peptidase B	0.43	0.019	0.54	0.031	23.3%	n.a.	10/3
Host/drug-resistance/secretion	K18145	adeA, multidrug efflux membrane fusion	-0.72	0.015	-0.61	0.012	23.3%	n.a.	1/4
Host/drug-resistance/secretion	K13792	ospG, secreted effector	-1.73	0.022	-0.51	0.046	20.0%	4	10/6
VFA/energy	K14940	cofF, gamma-F420-2 ligase	-1.23	0.022	-0.6	0.014	20.0%	30	10/6
Host/drug-resistance/secretion	K00856	adoK, adenosine kinase	-0.66	0.033	-0.57	0.020	16.7%	n.a.	6/6
Transport/two-component/N	K06857	tupC/vupC, tungstate transport ATP-binding	-1.52	0.005	-0.54	0.030	13.3%	5	10/6
Transport/two-component/N	K00362	nirB, nitrite reductase (NADH) large	0.80	0.011	0.61	0.012	13.3%	n.a.	10/6
Host/drug-resistance/secretion	K06237	COL4A, collagen type IV alpha	-0.13	0.015	-0.51	0.041	13.3%	1 (eukaryote-derived)	1/4
Transport/two-component/N	K00373	narJ/narW, nitrate reductase cofactor chaperone	-1.14	0.034	-0.59	0.015	13.3%	2	8/6
Host/drug-resistance/secretion	K19710	E2.7.7.53, ATP adenylyltransferase	-1.81	0.031	-0.54	0.029	13.3%	4	9/6
Amino-acid/vitamin	K01916	nadE, NAD+ synthase	-0.64	0.042	-0.6	0.014	13.3%	63	10/6
Carbohydrate utilization	K07026	E3.1.3.70, mannosyl-3-phosphoglycerate phosphatase	0.32	0.014	0.69	0.003	13.3%	n.a.	7/0
Amino-acid/vitamin	K01583	E4.1.1.19, arginine decarboxylase	-0.69	0.042	-0.52	0.037	13.3%	2	9/6
VFA/energy	K00192	cdhA, CODH/ACS subunit alpha	-0.27	0.005	-0.6	0.015	13.3%	n.a.	0/4

Module	KO	Annotation	log2FC	P(group)	rho_ADG	P(ADG)	Lasso freq.	Supporting genes (n)	Detection (low-FCR/high-FCR)
Carbohydrate utilization	K01690	edd, phosphogluconate dehydratase	0.48	0.034	0.63	0.008	10.0%	n.a.	9/4
Host/drug-resistance/secretion	K11893	impJ/vasE, type VI secretion	-0.66	0.031	-0.52	0.037	10.0%	2	10/6
Carbohydrate utilization	K02446	glpX, fructose-1,6-bisphosphatase II	0.53	0.005	0.56	0.024	10.0%	n.a.	10/6
Transport/two-component/N	K15600	thiZ, HMP transporter ATP-binding	0.53	0.000	0.55	0.026	10.0%	n.a.	10/6
Host/drug-resistance/secretion	K16648	aftD, arabinofuranan arabinosyltransferase	-0.98	0.000	-0.7	0.002	6.7%	1	9/6
Amino-acid/vitamin	K05275	E1.1.1.65, pyridoxine 4-dehydrogenase	-0.81	0.022	-0.72	0.002	3.3%	1	10/6
Host/drug-resistance/secretion	K03227	yscS/sctS, type III secretion S	-1.36	0.042	-0.55	0.029	3.3%	n.a.	5/6
Amino-acid/vitamin	K21721	sbnB, glutamate dehydrogenase	1.00	0.042	0.67	0.004	3.3%	8	10/6
Amino-acid/vitamin	K02549	menC, o-succinylbenzoate synthase	0.93	0.002	0.54	0.033	3.3%	1	10/5
VFA/energy	K01734	mgsA, methylglyoxal synthase	0.63	0.022	0.52	0.039	3.3%	65	10/6
Host/drug-resistance/secretion	K05363	murM, peptidoglycan serine/alanine adding enzyme	-1.59	0.011	-0.54	0.033	3.3%	34	10/6
Carbohydrate utilization	K00689	gtfB_C_D, dextransucrase	0.54	0.016	0.59	0.015	0.0%	13	10/6
Transport/two-component/N	K00374	narI/narV, nitrate reductase gamma	-1.16	0.042	-0.57	0.022	0.0%	1	10/6
Amino-acid/vitamin	K00899	mtnK, 5-methylthioribose kinase	-0.97	0.011	-0.57	0.020	0.0%	4	10/6

Table 3

The three metagenome-assembled genomes (MAGs) showing double evidence (between-group difference and ADG correlation). All are enriched in the high-FCR (inefficient) group and negatively correlated with ADG. As for the KO layer, these counts were not calibrated against a permutation null.

MAG	GTDB taxonomy (genus-level)	P(group)	log2FC	rho_ADG	P(ADG)
S8C510	Bacteria; Firmicutes_C; Negativicutes; Selenomonadales; Selenomonadaceae; g__UBA7018 (genus, unnamed)	0.031	-6.82	-0.70	0.003
S15C315	Bacteria; Bacteroidota; Bacteroidia; Bacteroidales; Muribaculaceae; g__Sodaliphilus (genus, unnamed)	0.031	-2.22	-0.57	0.021
S15C303	Bacteria; Firmicutes; Bacilli; RF39; UBA660; g__RUG12783 (genus, unnamed)	0.042	-4.50	-0.50	0.049

Statistical power of the design. The median pooled within-group standard deviation was 0.75 on the log2 scale. At the realised design of 10 versus 6 animals, the probability of detecting a true difference at $P < 0.05$ was 33.9% for a 1.5-fold change, 61.4% for two-fold, 91.6% for four-fold, and the smallest fold change reaching 80% nominal power was 3.0-fold. After Bonferroni correction for 3,283 tests, power at the realised design was < 0.1% even for a two-fold difference. The |log2 fold change| observed among the 36 candidates had a median of 0.20 (1.15-fold), well below what this design could detect. These figures define the ceiling of what this cohort could have shown: the null result should be read as "no effect large enough to be detected with 16 animals", not as "no effect", and it does not exclude differences of the modest magnitude usually reported for rumen functional genes. In the same simulation, 40 + 40 animals would give 96.5% nominal power (66.8% after Bonferroni correction) for a two-fold difference, which is the scale a definitive test of this hypothesis would require. Table 4 converts these calculations into the sample size a future study would need, expressed as animals per group for 80% power at each effect size.

Table 4. Animals per group required for 80% power at the within-group variation observed here (median pooled SD = 0.75 on the log2 scale), for a two-group comparison at each target fold change. The Bonferroni column uses alpha = 0.05/3,283, the threshold that would be needed for a KO-level screen of this size to be interpretable without a separate permutation calibration.

Target fold change	log2 fold change	Animals per group (nominal P < 0.05)	Animals per group (Bonferroni, 3,283 tests)	Total animals (Bonferroni)
1.25x	0.32	85	287	574
1.5x	0.58	26	87	174
2x	1.00	9	30	60
3x	1.58	4	12	24
4x	2.00	3	8	16

Discussion

In this rumen metagenome comparison of Tan sheep divergent in ADG, the interpretable result is a negative one. Neither overall community composition nor any individual KO distinguished the groups at a level that survived calibration: no KO approached FDR significance, the number of candidates returned by the two-layer screen did not exceed its permutation null, and a classifier built on those candidates did not generalise once feature selection was placed inside cross-validation. The functional axis suggested by the nominal ranking - sugar transport (chiG K17246, agaB K10984) and central energy metabolism (glpX K02446, K07026) in the faster-growing animals - is consistent with the literature, and we report it as a prioritized, testable list, but the present data do not establish it. We consider the quantification of selection leakage to be the most transferable finding: the same pipeline scored AUC = 1.000 when features were chosen on all animals and AUC = 0.767 when they were not.

Our findings align with a recurring, if sometimes under-appreciated, pattern in the literature. Pioneering work in cattle showed that high- and low-efficiency animals often do not differ in global community structure yet do differ in energy-harvesting capacity, with efficient animals enriched for ABC transporters, two-component systems, and amino-acid metabolism [3-5,32]. Later gene-centric and integrated meta-omics studies converged on the same functional axes - sugar transporters, PTS, two-component systems and amino-acid pathways - across beef cattle, dairy cows and sheep [8-12, 15]. The most directly comparable study, conducted in Hu sheep, likewise reported that gut microbiota co-vary with feed-conversion efficiency through coordinated host-microbe interactions [1], and multi-omics work in sheep pointed to the rumen microbiome as a co-regulator of efficiency [2]. Crucially, the specific genus names attached to these functions are unstable: Prevotella, Succinivibrionaceae and other taxa have moved in different directions across diets, breeds, laboratories and host species [3, 11]. Gene- and genome-level framing is more transportable because it keys on the catalytic function rather than on a name, and it is consistent with the inconsistent taxonomic reports across studies.

The closest direct comparator, a multi-omics study of Hu sheep published during preparation of this manuscript [1], combined rumen metagenomics with host multi-organ transcriptomics in 13 low-FCR versus 13 high-FCR lambs selected from a cohort of 150, and reported functional convergence on amino-acid biosynthesis, central carbon metabolism and propionate-oriented fermentation, with carbohydrate-active enzyme modules (GH126, CBM27, EPS-GT) enriched in efficient animals. The convergent picture across that study and ours - carbohydrate and energy remodelling rather than wholesale community change - is encouraging, but the two studies differ in scope and positioning. First, the design of [1] (larger screening cohort, host transcriptomics, and rumen fermentation end-products) resolves mechanistic questions that a 16-animal, single-omics design cannot address; its pathway-level conclusions should therefore be regarded as the current mechanistic standard for sheep. Second, the present study contributes breed-level evidence in Tan sheep, an indigenous Chinese breed managed under a commercial high-forage finishing system, and - importantly for translational use - distils the signal into an explicit, testable 36-KO panel (Table 2 and Supplementary Table S1) plus three genome-resolved MAG anchors. Given the permutation results above, that panel should be read as a list of targets to be tested, not as a validated biomarker set. We therefore frame our contribution not as a competing mechanistic claim but as an independent, gene-level candidate resource that (i) corroborates the carbohydrate-uptake and energy-metabolism axis in a second breed and (ii) provides named, assay-ready targets for validation in larger cohorts. Determining whether the panel generalises across breeds and diets will require host-transcriptomic and fermentation-phenotype integration of the kind achieved by [1] and by dairy-cow meta-omics [12].

The three double-evidence MAGs are notable because they were all inefficient-enriched, negatively correlated with growth, and assignable only to genus-level, currently unnamed lineages - two Firmicutes-affiliated genomes (Selenomonadaceae UBA7018; UBA660/RF39 RUG12783) and one Bacteroidota-affiliated genome (Muribaculaceae Sodaliphilus). Their direction is internally coherent: animals with slower growth harboured more of these uncharacterized lineages. Rather than over-interpreting the genus labels, which reflect incomplete reference databases, we regard them as genome-resolved anchors for the functional modules identified at KO level. They echo reports that a handful of heritable, phylogenetically coherent rumen taxa are linked to host energy harvesting [4, 13], and they illustrate how binning can recover ecologically relevant, previously unannotated organisms that would be invisible to genus-level reference mapping [20].

From an applied standpoint, the 36 KOs listed in Table 2 - and especially the Lasso-stable K17246 chitobiose permease, K10780 fabL and K10984 agaB - are best used as a candidate microbial biomarker panel to be tested, not as a validated one. The non-nested model discriminated the groups perfectly on AUC (1.000) and assigned 14 of 16 animals correctly, but this performance was manufactured by selecting features on the same animals used for evaluation; under nested validation the same pipeline gave AUC = 0.767 and 56.2% accuracy, not significantly better than permuted labels (P = 0.190). At 3,283 features and 16 animals, perfect separation is the expected outcome of a leaky design rather than evidence of a biological signal. Any future panel of this kind should be developed with nested validation and confirmed by targeted ddPCR or qPCR in an independent cohort; methane and energy-loss dimensions should also be monitored [27-30], and causality will require controlled validation.

This study has several limitations. First, the sample size is small and unbalanced (n = 10 versus n = 6), and Benjamini-Hochberg correction yielded no significant hits (smallest adjusted P = 0.41); more importantly, a label-permutation calibration showed that the candidate counts themselves - 54, 94 and 36 at the three layers - are within, or below, what random relabelling of these 16 animals produces. The power analysis quantifies the consequence: at 10 versus 6 animals this design could only detect differences of about three-fold or more at nominal thresholds, and effectively nothing after correction for 3,283 tests, whereas the fold changes actually observed among the candidates had a median of 1.15-fold. The null result therefore constrains the size of any true effect rather than demonstrating that no effect exists. Second, efficiency groups were defined by ADG rather than by directly measured individual FCR, because individual feed intake was not recorded; all lambs received the same diet with negligible between-pen intake variation (1,576 +/- 38 g/d), so ADG is a reasonable proxy under iso-intake conditions, but the observed two-fold ADG contrast is larger than the 10-30% efficiency differences typically reported between divergent groups, and the absence of any animal with an ADG between 198 and 301 g/d means unrecorded differences in intake, pen or developmental stage cannot be excluded. Direct FCR-based grouping would require individual intake records. Selecting the two tails of a 100-animal cohort maximised the phenotypic contrast obtainable at this sample size, which makes the absence of any surviving signal harder to attribute to insufficient contrast; conversely, effect sizes estimated between such extremes are not population averages. Third, initial body weight differed between groups (31.51 versus 26.92 kg) and was correlated with ADG (rho = 0.67, P = 0.005); candidate KOs were also correlated with initial weight (median |rho| = 0.39 versus 0.59 for ADG), so body size is a plausible partial confounder that this design cannot remove. Fourth, several candidate KOs are supported by only one or two catalogue genes, so their abundance estimates are intrinsically unstable; the number of supporting genes is reported in Table 2 and should be used to prioritise targets. Fifth, the design is observational and associative. Sixth, the three key MAGs are unnamed at genus level and gene-level taxonomic attributions are LCA-based predictions. Seventh, we lack metatranscriptomics and did not measure rumen VFA concentrations or methane flux. Finally, the panel requires independent validation in an external, larger cohort with targeted qPCR/ddPCR and, ideally, cultivation or microbiota-inoculation experiments of the kind that have established causal roles for propionate-producing rumen genomes in lambs [31].

Conclusion

In finishing Tan sheep, divergence in growth rate was not associated with any statistically detectable difference in rumen functional genes: the carbohydrate-uptake and energy-metabolism candidates that emerge from a nominal two-layer screen did not exceed permutation-based null expectations, no KO approached FDR significance, and no classifier built on them generalised under nested validation. What the study does provide is a breed-specific genome resource (591 MAGs, including three unnamed, growth-associated lineages) for Tan sheep under a high-forage finishing system, a prioritized list of targets for independent validation, and a concrete measurement of how much apparent signal non-nested feature selection can create at this sample size. The power analysis adds a design target: at the within-group variation observed here, a study intending to detect a two-fold difference with correction for 3,283 tests would need about 30 animals per group, whereas a realistic 1.5-fold effect would need about 87 per group (Table 4). Until cohorts of that size are assembled, rumen functional-gene screens in sheep should be read as hypothesis-generating rather than confirmatory.

Declarations

Ethics approval and consent to participate: All animal procedures were approved by the Science and Technology Ethics Committee of Ningxia University (approval no. NXU-2025-309). Informed consent was obtained from the owners of all animals used in this study. Animals were slaughtered humanely according to standard commercial slaughter procedures at the experimental farm, and rumen contents were collected immediately after slaughter.

Consent for publication: Not applicable.

Availability of data and materials: The metagenomic sequencing data have been deposited in the NCBI Sequence Read Archive (SRA) under BioProject accession PRJNA1531002 (Study: SRP737645). The 16 samples are accessible under SRR40722286, SRR40722287, SRR40722288, SRR40722289, SRR40722290, SRR40722291, SRR40722292, SRR40722293, SRR40722294, SRR40722295, SRR40722296, SRR40722297, SRR40722298, SRR40722299, SRR40722300, and SRR40722301. All analysis scripts for the differential-abundance screen, the permutation calibration, the nested cross-validation and the power analysis are available from the corresponding author on reasonable request and will be

deposited in the Science Data Bank (ScienceDB, https://www.scidb.cn), a general-purpose repository recommended by Springer Nature that assigns a permanent DOI and CSTR identifier, prior to publication. Derived abundance tables, candidate lists, host-filtering statistics and MAG quality statistics are provided as Supplementary Tables S1-S3.

Competing interests: The authors declare that they have no competing interests.

Funding: This work was supported by the Key Research and Development Program of Ningxia Hui Autonomous Region (grant no. 2024BBF01010). The funding body played no role in the design, analysis or writing of the study.

Authors' contributions (CRediT): Jin Wang: Conceptualization, Data curation, Formal analysis, Investigation, Methodology, Visualization, Writing - original draft. Jifeng Ma: Conceptualization, Funding acquisition, Project administration, Resources, Supervision, Writing - review & editing. Yu Fan: Methodology, Software, Validation, Visualization. Huiming Zhang: Resources, Supervision, Writing - review & editing. Qing Ma: Investigation, Resources, Data curation. Xuansheng Li: Investigation, Methodology, Writing - review & editing.

Acknowledgements: We thank the staff of Nuanquan Sheep Farm for assistance with animal management and sampling, and Tsingke Biotechnology Co., Ltd. for sequencing services.

References

1. Jia X et al. Integrative analysis of rumen microbiota and host multi-organ interactions underlying feed conversion efficiency in Hu sheep. J Anim Sci Biotechnol. 2026;17:19. 10.1186/s40104-025-01333-3. PMID: 41630069.
2. Zhou G et al. Multi-omics revealed the mechanism of feed efficiency in sheep by the combined action of the host and rumen microbiota. Anim Nutr. 2024;18:367–379. 10.1016/j.aninu.2024.04.009. PMID: 39290858.
3. Shabat SK, Sasson G, Doron-Faigenboim A et al. Specific microbiome-dependent mechanisms underlie the energy harvest efficiency of ruminants. ISME J. 2016;10(12):2958–2972. 10.1038/ismej.2016.62. PMID: 27152936.
4. Sasson G, Ben-Shabat SK, Seroussi E et al. Heritable bovine rumen bacteria are phylogenetically related and correlated with the cow's capacity to harvest energy from its feed. mBio. 2017;8(4):e00703-17. 10.1128/mBio.00703-17. PMID: 28811339.
5. Myer PR, Wells JE, Smith TPL, Kuehn LA, Freetly HC. Rumen microbiome from steers differing in feed efficiency. PLoS One. 2015;10(6):e0129174. 10.1371/journal.pone.0129174. PMID: 26030887.
6. Hess M, Sczyrba A, Egan R et al. Metagenomic discovery of biomass-degrading genes and genomes from cow rumen. Science. 2011;331(6016):463–467. 10.1126/science.1200387. PMID: 21273488.
7. Brulc JM, Antonopoulos DA, Berg Miller ME et al. Gene-centric metagenomics of the fiber-adherent bovine rumen microbiome reveals forage specific glycoside hydrolases. Proc Natl Acad Sci USA. 2009;106(6):1948–1953. 10.1073/pnas.0806191105. PMID: 19181843.
8. Li F, Hitch TCA, Chen Y et al. Comparative metagenomic and metatranscriptomic analyses reveal the breed effect on the rumen microbiome and its associations with feed efficiency in beef cattle. Microbiome. 2019;7:6. 10.1186/s40168-019-0618-5. PMID: 30642389.
9. Auffret MD, Stewart RD, Dewhurst RJ et al. Identification of microbial genetic capacities and potential mechanisms within the rumen microbiome explaining differences in beef cattle feed efficiency. Front Microbiol. 2020;11:1229. 10.3389/fmicb.2020.01229. PMID: 32582125.
10. Lima J, Auffret MD, Stewart RD et al. Identification of rumen microbial genes involved in pathways linked to appetite, growth, and feed conversion efficiency in cattle. Front Genet. 2019;10:701. 10.3389/fgene.2019.00701. PMID: 31440274.
11. Xue MY, Sun HZ, Wu XH, Liu JX, Guan LL. Multi-omics reveals that the rumen microbiome and its metabolome together with the host metabolome contribute to individualized dairy cow performance. Microbiome. 2020;8(1):64. 10.1186/s40168-020-00819-8. PMID: 32398126.
12. Xue MY, Xie YY, Zhong Y et al. Integrated meta-omics reveals new ruminal microbial features associated with feed efficiency in dairy cattle. Microbiome. 2022;10(1):32. 10.1186/s40168-022-01228-9. PMID: 35172905.
13. Tapio M, Fischer D, Mantysaari P, Tapio I. Rumen microbiota predicts feed efficiency of primiparous Nordic Red dairy cows. Microorganisms. 2023;11(5):1116. 10.3390/microorganisms11051116. PMID: 37317090.
14. Clemmons BA, Voy BH, Embree MM et al. Rumen bacteria and serum metabolites predictive of feed efficiency phenotypes in beef cattle. Sci Rep. 2019;9:19265. 10.1038/s41598-019-55978-y. PMID: 31848455.
15. Shi W, Moon CD, Leahy SC et al. Methane yield phenotypes linked to differential gene expression in the sheep rumen microbiome. Genome Res. 2014;24(9):1517–1525. 10.1101/gr.168245.113. PMID: 24907284.
16. Li D, Liu CM, Luo R, Sadakane K, Lam TW. MEGAHIT: an ultra-fast single-node solution for large and complex metagenomics assembly via succinct de Bruijn graph. Bioinformatics. 2015;31(10):1674–1676. 10.1093/bioinformatics/btv033. PMID: 25609793.

17. Huerta-Cepas J, Szklarczyk D, Forslund K et al. eggNOG 4.5: a hierarchical orthology framework with improved functional annotations for eukaryotic, prokaryotic and viral sequences. Nucleic Acids Res. 2016;44(D1):D286-D293. 10.1093/nar/gkv1248. PMID: 26582926.
18. Nissen JN, Johansen J, Allesoee RL et al. Improved metagenome binning and assembly using deep variational autoencoders. Nat Biotechnol. 2021;39(5):555–560. 10.1038/s41587-020-00777-4. PMID: 33398153.
19. Parks DH, Imelfort M, Skennerton CT, Hugenholtz P, Tyson GW. CheckM: assessing the quality of microbial genomes recovered from isolates, single cells, and metagenomes. Genome Res. 2015;25(7):1043–1055. 10.1101/gr.186072.114. PMID: 25977477.
20. Stewart RD, Auffret MD, Warr A et al. Assembly of 913 microbial genomes from metagenomic sequencing of the cow rumen. Nat Commun. 2018;9(1):870. 10.1038/s41467-018-03317-6. PMID: 29491419.
21. Love MI, Huber W, Anders S. Moderated estimation of fold change and dispersion for RNA-seq data with DESeq2. Genome Biol. 2014;15(12):550. 10.1186/s13059-014-0550-8. PMID: 25516281.
22. Robinson MD, McCarthy DJ, Smyth GK. edgeR: a Bioconductor package for differential expression analysis of digital gene expression data. Bioinformatics. 2010;26(1):139–140. 10.1093/bioinformatics/btp616. PMID: 19910308.
23. Mallick H, Rahnavard A, McIver LJ et al. Multivariable association discovery in population-scale meta-omics studies. PLoS Comput Biol. 2021;17(11):e1009442. 10.1371/journal.pcbi.1009442. PMID: 34784344.
24. Pasolli E, Truong DT, Malik F, Waldron L, Segata N. Machine learning meta-analysis of large metagenomic datasets: tools and biological insights. PLoS Comput Biol. 2016;12(7):e1004977. 10.1371/journal.pcbi.1004977. PMID: 27400279.
25. Uritskiy GV, DiRuggiero J, Taylor J. MetaWRAP - a flexible pipeline for genome-resolved metagenomic data analysis. Microbiome. 2018;6(1):158. 10.1186/s40168-018-0541-1. PMID: 30219103.
26. Segata N, Izard J, Waldron L et al. Metagenomic biomarker discovery and explanation. Genome Biol. 2011;12(6):R60. 10.1186/gb-2011-12-6-r60. PMID: 21702898.
27. Roehe R, Dewhurst RJ, Duthie CA et al. Bovine host genetic variation influences rumen microbial methane production with best selection criterion for low methane emitting and efficiently feed converting hosts based on metagenomic gene abundance. PLoS Genet. 2016;12(2):e1005846. 10.1371/journal.pgen.1005846. PMID: 26891056.
28. Zhou M, Hernandez-Sanabria E, Guan LL. Assessment of the microbial ecology of ruminal methanogens in cattle with different feed efficiencies. Appl Environ Microbiol. 2009;75(20):6524–6533. 10.1128/AEM.02815-08. PMID: 19717632.
29. Wallace RJ, Rooke JA, McKain N et al. The rumen microbial metagenome associated with high methane production in cattle. BMC Genomics. 2015;16:839. 10.1186/s12864-015-2032-0. PMID: 26494241.
30. Hook SE, Wright ADG, McBride BW. Methanogens: methane producers of the rumen and mitigation strategies. Archaea. 2010;2010:945785. 10.1155/2010/945785. PMID: 21253540.
31. Chen T, Yu S, Li K et al. Rumen microbiota inoculation indicates collaborative mechanisms enhancing propionate supply to alleviate weaning stress in lambs. Microbiome. 2026;14:54. 10.1186/s40168-025-02283-8. PMID: 41491581.
32. Zhou X, Cai Z, Zeng Y et al. Rumen and fecal microbiota characteristics of Qinchuan cattle with divergent residual feed intake. Microorganisms. 2023;11(2):358. 10.3390/microorganisms11020358. PMID: 36838323.
33. Hyatt D, Chen GL, Locascio PF, Land ML, Larimer FW, Hauser LJ. Prodigal: prokaryotic gene recognition and translation initiation site identification. BMC Bioinformatics. 2010;11:119. 10.1186/1471-2105-11-119. PMID: 20211023.
34. Fu L, Niu B, Zhu Z, Wu S, Li W. CD-HIT: accelerated for clustering the next-generation sequencing data. Bioinformatics. 2012;28(23):3150–3152. 10.1093/bioinformatics/bts565. PMID: 23060610.
35. Langmead B, Salzberg SL. Fast gapped-read alignment with Bowtie 2. Nat Methods. 2012;9(4):357–359. 10.1038/nmeth.1923. PMID: 22388286.
36. Buchfink B, Xie C, Huson DH. Fast and sensitive protein alignment using DIAMOND. Nat Methods. 2015;12(1):59–60. 10.1038/nmeth.3176. PMID: 25402007.
37. Chen S, Zhou Y, Chen Y, Gu J. fastp: an ultra-fast all-in-one FASTQ preprocessor. Bioinformatics. 2018;34(17):i884-i890. 10.1093/bioinformatics/bty560. PMID: 30423086.

Figures

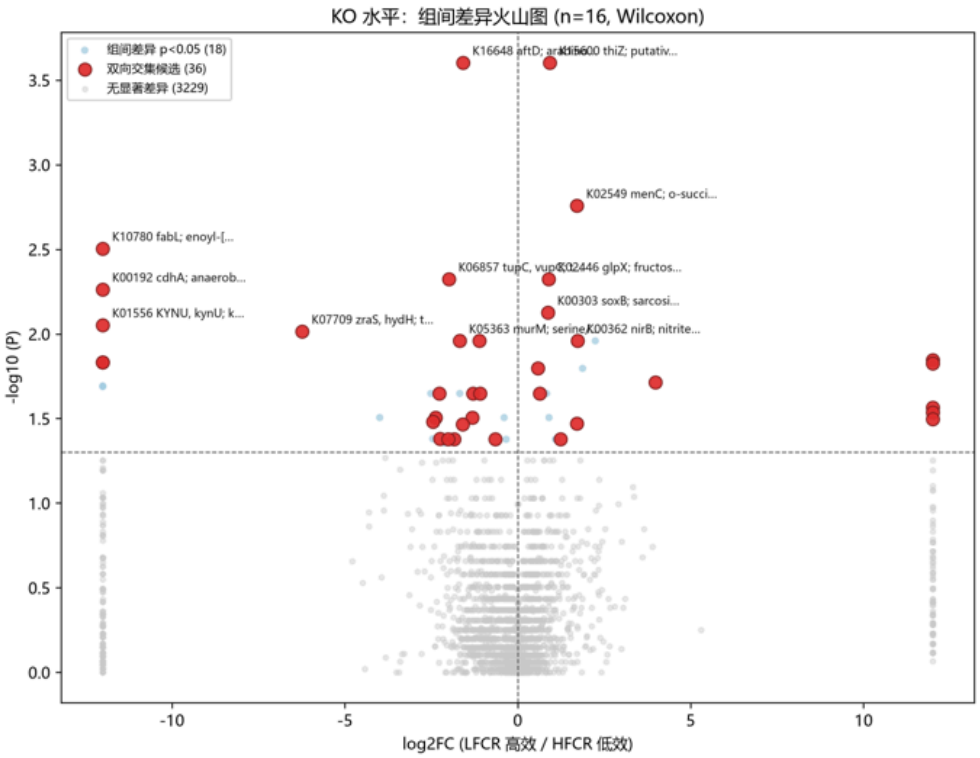


Figure 1

Figure 1

Volcano plot of between-group KO differences (low-FCR versus high-FCR). Each point is one of 3,283 tested KOs; colour denotes significance of the Wilcoxon between-group test (P < 0.05) and symbol size encodes magnitude of the ADG correlation. The 36 nominal candidates are highlighted; the number of such points should be read against the permutation null reported in the text.

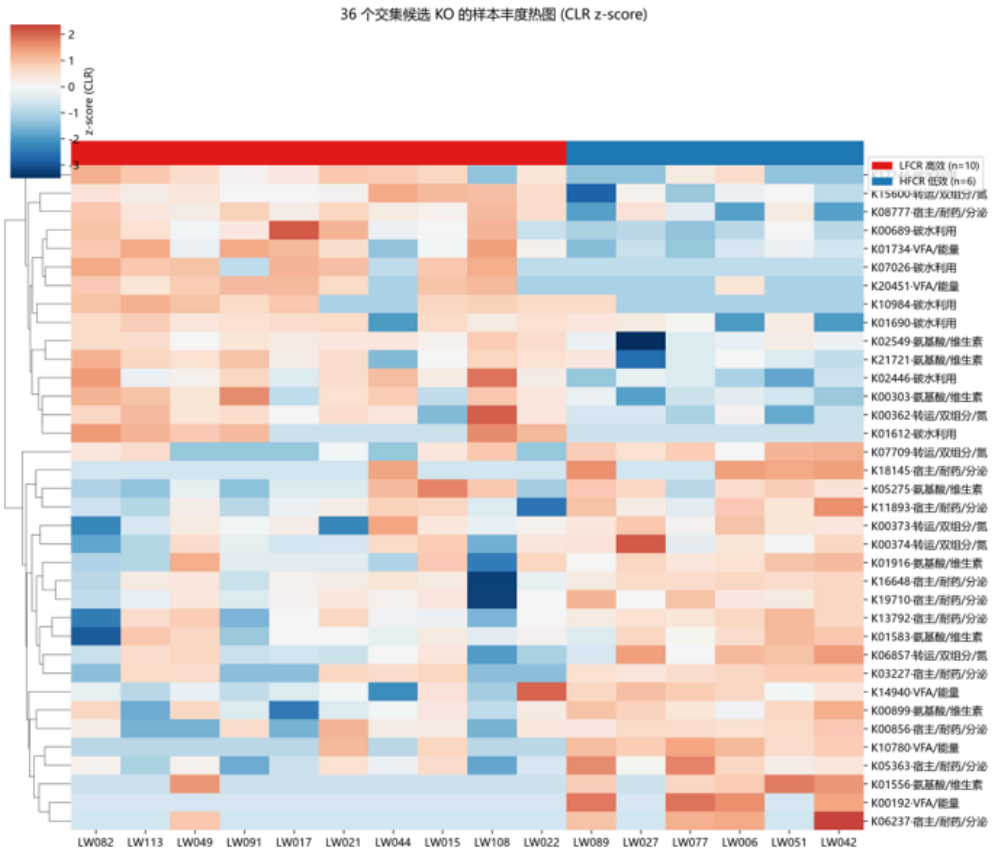


Figure 2

Figure 2

Heat map of the 36 double-evidence candidate KOs across the 16 Tan sheep, with samples clustered by phenotype group (low-FCR efficient group; high-FCR inefficient group). Rows are KOs and columns are animals, scaled by within-KO abundance.

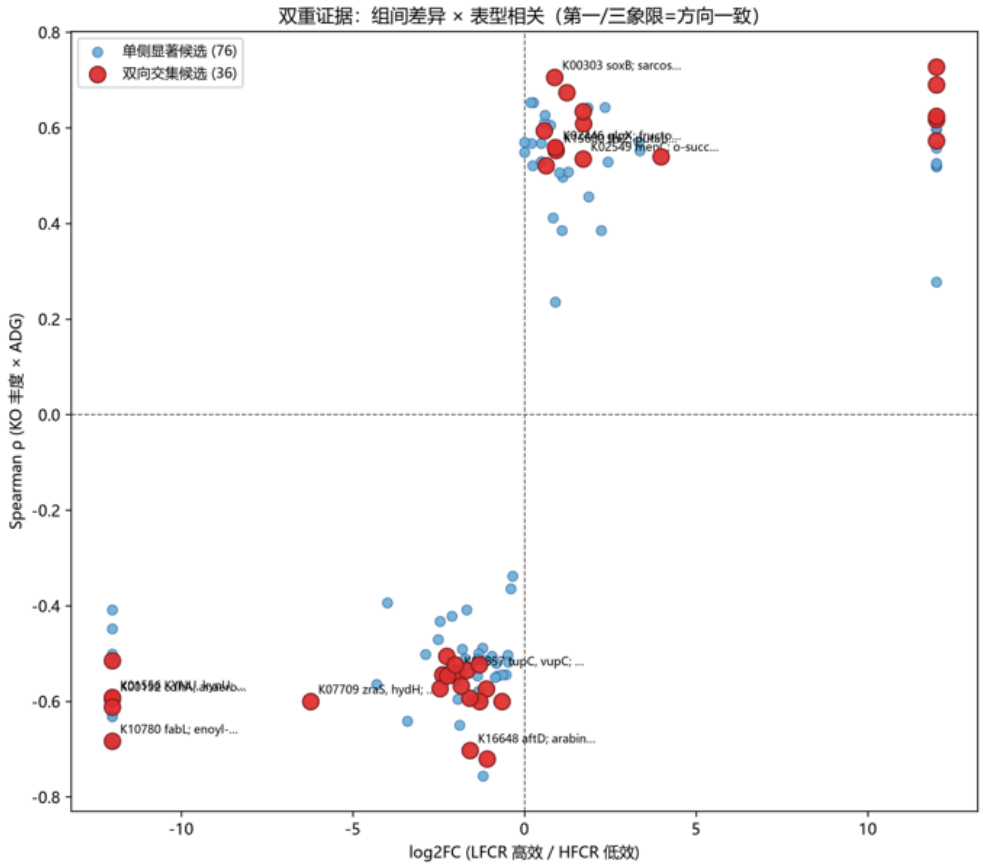


Figure 3

Figure 3

Double-evidence scatter plot. The x-axis shows the between-group log2 fold change (low-FCR/high-FCR) and the y-axis shows the Spearman correlation with ADG (rho) for each KO. Points in the upper-right and lower-left quadrants with both P < 0.05 are the 36 direction-concordant candidates; their quadrant alignment reflects the concordance criterion of the screen, which is a selection rule rather than an independent result.

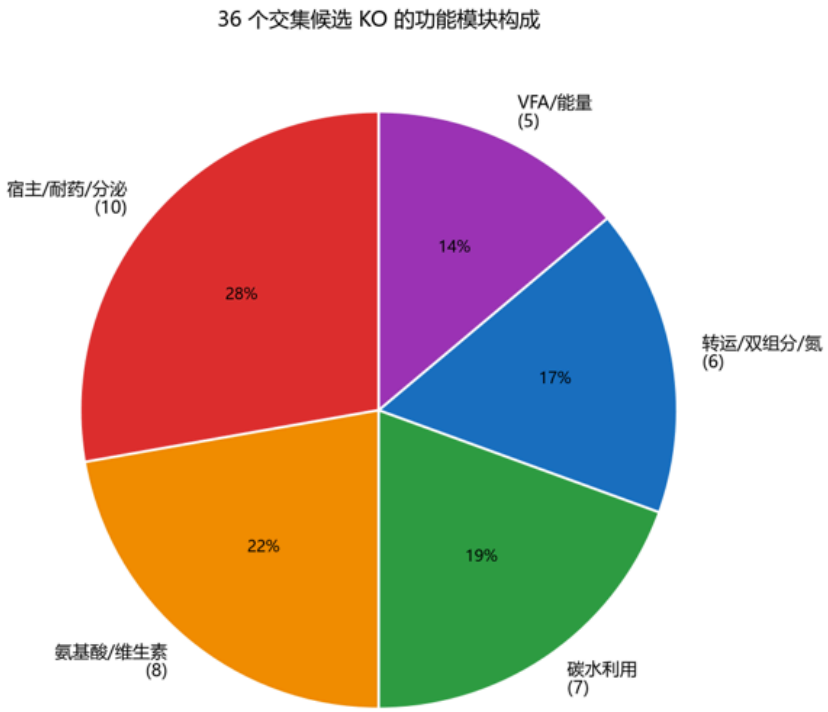


Figure 4

Figure 4

Functional-module composition of the 36 double-evidence candidate KOs: host/drug-resistance/secretion (10), amino-acid/vitamin (8), carbohydrate utilization (7), transport/two-component/nitrogen (6) and VFA/energy (5).

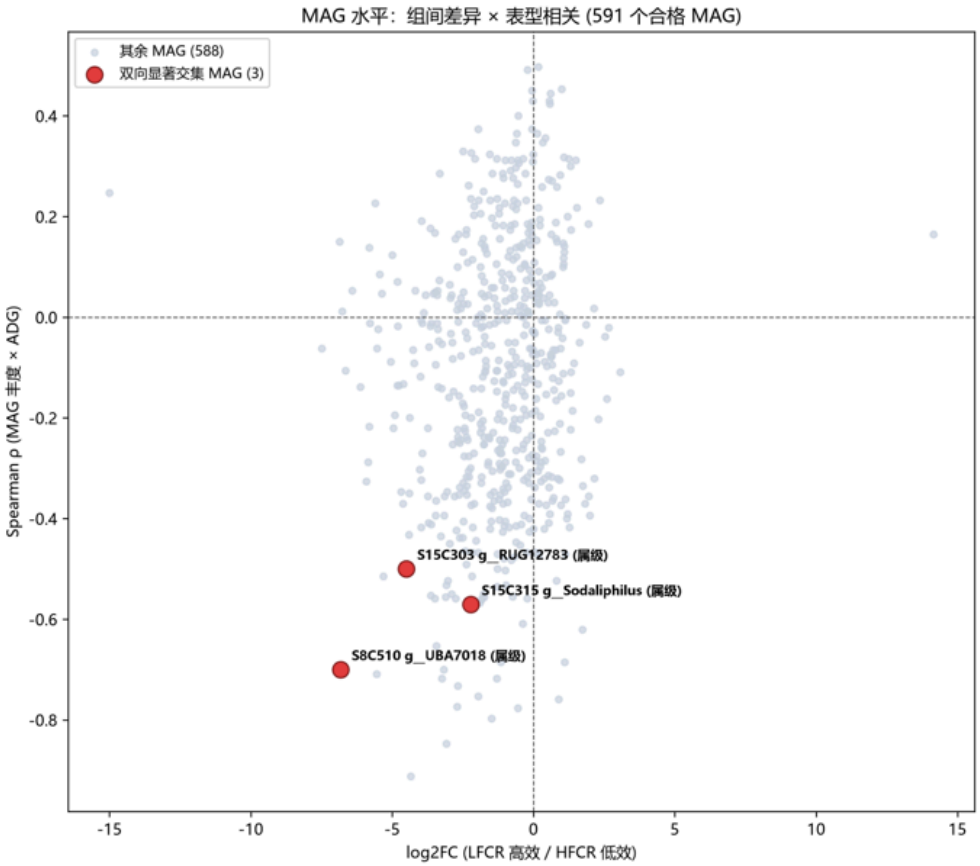


Figure 5

Figure 5

Scatter plot of the 591 qualified MAGs, plotting between-group significance against ADG correlation. The three double-evidence MAGs (S8C510, S15C315, S15C303), all enriched in the high-FCR group and negatively correlated with ADG, are labelled with their genus-level GTDB assignment.